

RSC Advances



This is an *Accepted Manuscript*, which has been through the Royal Society of Chemistry peer review process and has been accepted for publication.

Accepted Manuscripts are published online shortly after acceptance, before technical editing, formatting and proof reading. Using this free service, authors can make their results available to the community, in citable form, before we publish the edited article. This *Accepted Manuscript* will be replaced by the edited, formatted and paginated article as soon as this is available.

You can find more information about *Accepted Manuscripts* in the [Information for Authors](#).

Please note that technical editing may introduce minor changes to the text and/or graphics, which may alter content. The journal's standard [Terms & Conditions](#) and the [Ethical guidelines](#) still apply. In no event shall the Royal Society of Chemistry be held responsible for any errors or omissions in this *Accepted Manuscript* or any consequences arising from the use of any information it contains.

An immobilization multienzyme microfluidic chip for acetylcholinesterase inhibition assay by fluorescence method

Yulan Tang¹, Sufang Liu^{2*}, Rongbiao Pi¹, Zhiyi Cheng^{1†}

1. *School of Pharmaceutical Sciences, Sun Yat-Sen University, Guangzhou 510006, China*

2. *School of Public Health, Sun Yat-Sen University, Guangzhou 510080, China*

* Corresponding author. *E-mail:* liusf@mail.sysu.edu.cn. *Tel:* +86 020 87332517.

† Corresponding author. *E-mail:* chengzhy@mail.sysu.edu.cn. *Tel:* +86 020 39943047.

Abstract

A bi-enzymes immobilized microfluidic device was developed for the rapid enzyme inhibition assay by fluorescence detection. The micro-channels of chip were activated by using an acidic hydrogen peroxide (H_2O_2) solution, followed by amination with 3-aminopropyltriethoxysilane / methyltriethoxysilane (APTES / MTES) mixture, and then followed by glutaraldehyde grafting and subsequent covalent protein binding. The analysis was based on the oxidation of L-tyrosine to its tyrosine dimer in the presence of horseradish peroxidase (HRP) and H_2O_2 , which has maximal excitation and emission wavelengths at 320 nm and 416 nm, respectively. H_2O_2 was an end product under the catalysis of acetylcholinesterase (AChE) and choline oxidase (ChO) immobilized on inner surface of a microchip, using acetylcholine (ACh) as enzyme substrate. Fluorescence of the dimer was directly proportional to the concentration of the H_2O_2 and partly reflected enzyme activity. Thus, AChE inhibition activity was indicated by a decrease in fluorescence signal detected by microplate reader. The effects of flow velocities, reaction time and buffer systems (pH, types and concentration) on the reaction system were investigated. The utility of the developed microchip was demonstrated for AChE inhibition studies using Donepezil as a model compound, which relied upon the generation of a uniform concentration of substrate and a microfluidically created concentration gradient of inhibitor using a single initial inhibitor concentration. The IC_{50} value of Donepezil was determined and found to correlate well with that obtained in microplate. Accordingly, the microchip can be applied to the screening of enzyme inhibitor and

enzymatic reaction kinetics study, which may be useful for drug discovery and screening.

Keywords: Microfluidic chip; Immobilized enzymes; Acetylcholinesterase; Enzyme inhibition assay; Fluorescence detection

Introduction

Alzheimer's disease (AD), which is the most prevalent form of dementia and has become a major public health concern to societies worldwide. According to the cholinergic hypothesis, low levels of ACh in the brain is a significant factor in AD^{1,2}. AChE is serine hydroxylase classically associated with the hydrolysis of the neurotransmitter ACh and responsible for regulating the level of ACh in the nerve system³. Furthermore, it is reported that AChE is related to many neurological disorders⁴. Accordingly, AChE is currently indicated as a prime target enzyme for drugs to be used in the treatment of patients diagnosed with AD^{5,6}. Currently, five drugs have been approved by the U.S. Food and Drug Administration (FDA) to treat AD, such as Donepezil (ARICEPT[®]), Galantamine (REMINYL[®]), Rivastigmine (EXELON[®]), Tacrine (COGNEX[®]) as well as the Memantine. The first four drugs are acetylcholinesterase inhibitors (AChEIs) and the last one is the N-methyl-D-aspartate receptor antagonist, they are proved to be effective against AD and can improve the life quality of the patients^{7,8}. Among them, Galantamine and Rivastigmine are of natural origin, which implies that natural plant pharmaceuticals have become an important resource for drug discovery^{9,10}. However, AChEIs available for the treatment of AD are inadequate and their uses are limited by serious adverse side

effects. Therefore, the search for new AChEIs has attracted a great deal of attention. It is well known that drug discovery is time-consuming process and expensive. For this reason, simple, fast, inexpensive and continuous analytical methods for improving its overall efficiency are quite necessary.

The development of an ultra sensitive and rapid technique for the screening of AChEIs is a topic of substantial interest in the biomedical, agricultural, environmental monitoring and food quality control domains ¹¹. So far, a series of methods for evaluating of therapeutic drugs regulating AD based on reduction of AChE activity are already published using the free or the immobilized enzyme. Most of these either use colorimetric, fluorometric, spectrophotometric, or electrochemical techniques ¹². Nevertheless, the most widely used method is based on a colorimetric method developed by Ellman and coworkers ¹³. Although the method is simple, accurate, and inexpensive, it may result in false-positive effect due to instability of the Ellman's reagent solution and the interaction with abundant free sulfhydryl (SH) groups in biological samples. Meanwhile, the use of non-physiological substrate different from ACh will have an effect on the measurement of inhibition constants. To solve the problem of the original Ellman's method, modified Ellman have been reported subsequently ^{14, 15}. It provided low background and high sensitivity in biological samples assay, but such a colorimetric method in microplates or test tubes was not only relatively laborious and time-consuming, and also large reagent consumption. In addition, various analytical methods based on co-immobilized target enzymes in biosensor and in microreactor configurations become one new trend in the field of

drug discovery and analysis, and have been generally investigated¹⁶⁻¹⁸. The benefits of co-immobilized multi-enzymatic systems are: co-immobilization compact distances between enzyme and reagent dramatically, and enhance the “global” efficiency of the enzyme catalytic reaction by the in-situ generation of its substrate. Furthermore, undesired by-products of an enzymatic reaction could be eliminated^{19,20}. Meanwhile, with rapid development of micrototal analysis system (μ -TAS), the microfluidic device offers excellent advantages in short assay times, reduced reagent consumption and cost, faster mixing as well as high throughput analysis capability compared to the traditional ml-scale systems²¹. Recently, combining the merits of co-immobilized multi-enzymatic systems and microfluidic device, a co-immobilized microfluidic enzyme reactors appear as a promising alternative to the classical methods for screening potential AChEIs²².

Over the last decades, various immobilization methods, such as physical adsorption and entrapment, covalent coupling, cross-linking, affinity absorption, self-assembled monolayer, have been proposed for constructing the immobilized enzyme reactors in the format of microfluidic chips²³ or capillaries²⁴ or other supports²⁵⁻²⁷. In general, all the above methods have their advantages and limitations²⁸. Covalent binding strategy generally ensures the highest strength of the bonding between enzyme and support, minimizing leakage issues. Hence, it is a more efficient method than simple physisorption²⁹. Among the covalent binding strategies, self-assembled monolayers (SAMs) is a promising technique and it has many advantages compared to others such as physical and bioaffinity immobilization^{30,31}. Currently, self-assembled monolayers

of organosilane have attracted researcher's interests and have been widely used to immobilize proteins on silicon and PDMS surfaces, because they formed stable and well-defined organic layers. In addition, surfaces with different properties can be easily prepared by using silane coupling reagents with different terminal groups^{32,33}. APTES is one of the most widely used organosilane agent for the preparation of amine-terminated surface. Moreover, the influence of experimental parameters on the quality of the APTES layer was investigated comprehensively³⁴. Both Wang³⁵ and Goyal³⁶ used mixed silane composition (APTES and MTES) for covalent immobilization of proteins to offer control over the spatial distribution of grafted APTES molecules and maintain more activity of enzyme during immobilization procedure. Such researches give us an inspiration in enzyme immobilization.

Thus far, although AChE has been actively investigated in varied fields by many researchers, its inhibitor screening on chip remain elusive. We are (to our knowledge) the first to introduce an eco-friendly and effective bi-enzymatic co-immobilized microfluidic chip with AChE and ChO for the analysis of AChE activity by fluorescence method. The bi-enzymatic co-immobilized device was modified by using mixed silanes (APTES / MTES), to form dense, self assembled monolayers and render medium hydrophobic internal surface for enzyme immobilization. The advantages of our co-immobilized enzymes chip over the conventional methods included low reagent consumption, simple operation and system automation, which allowed a large number of compounds to be assayed continuously. It was well suited for relevant high-throughput screening of AChEIs. In this context, optimum working

conditions of microfluidic chip with respect to the substrate concentration, reaction time and different kinds of buffer systems (pH and concentration) were investigated. Moreover, the Michaelis–Menten parameters (K_m and V_{max}) of the co-immobilized enzymes were compared with the free form. Under the optimum conditions, Donepezil, as a model AChEI, the IC50 value was determined and the performance of the chip was also evaluated. The co-immobilized enzymes chip can be expected to be an effective microfluidic tool for enzyme inhibitor screening.

Experimental

Reagents and apparatus

Sylgard184 silicone elastomer and curing agent were purchased from Dow Corning (Midland, MI, USA). AChE (EC 3.1.1.7, from *Electric eel*, 241 U·mg⁻¹), ChO (EC1.1.3.17, from *Alcaligenes species*, 14 U·mg⁻¹), acetylcholine chloride (AChCl), Donepezil hydrochloride were purchased from Sigma-Aldrich (St. Louis, MO, USA). L-tyrosine (C₉H₁₁NO₃) was obtained from Shanghai Bio Life Science & Technology Co. Ltd. (Shanghai, China). HRP (EC1.11.1.7, 250 U·mg⁻¹), H₂O₂ (30%, w/w, aqueous solution), APTES (99%), MTES(98%), glutaraldehyde (50%), tris(hydroxymethyl)aminomethane (Tris) and fluorescein sodium were all purchased from Aladdin (Shanghai, China). Phosphate buffer solution (PB, pH 8.0) was prepared by mixing KH₂PO₄ and Na₂HPO₄. Ultrapure water (18.4 MΩ) was purified by a Millipore Simplicity system (Millipore, Bedford, MA, USA) and used throughout all experiments. All other used chemicals were of analytical grades without further purification and obtained from common commercial supplies.

The buffer solutions were filtered through a 0.45 μm membrane filter and degassed before pumping into micro-channel. Reaction solutions were supplied to microreactor using a syringe pump (Model LSP02-1B, Longer Pump, Corporation, Baoding, China). A PDC-32G plasma generator from Harrick Plasma (Harrick Plasma, USA) was used to bond PDMS and glass chips. Portable bench drill was used to punch holes (TD-200, 2.5 mm diameter, Shanghai, China). Besides, we made a homemade joints by cutting a piece of the pipette tip (200 μL), which closely matched with the main inlet and polyethylene tubes, and the latter were used to further connect the main inlet with a syringe pump for sample delivery and washing. Fluorescence spectra and intensities were monitored at 25 $^{\circ}\text{C}$ with a FlexStation3 microplate reader (Molecular Devices, Shanghai, China)

Microfluidic chip design and fabrication

The microfluidic device has dimension of 6.8 \times 6.8 cm, and was composed of three-layer, as shown in Fig.1A. The top layer (layer a) and bottom layer (layer b) were fabricated from polydimethylsiloxane (PDMS) containing the micro-channels, and the middle one (layer c) was glass. The main functional regions of each layer were simply described below: (1) A fluid equivalent distributor, sinuous channels and detection windows were patterned on the top layer (part 3 and 4), the sinuous channels were a micromixer for fluorescence derivation. In addition, detection chambers were adapt to well architecture in the 96-microplate so that fluorescence intensity could be detected by a microplate reader; (2) Reaction chambers and concentration gradient generator were patterned on the bottom layer (part 1 and 2); (3)

Six parallel holes of the middle one were designed for connecting liquid flow and two holes at the same place of C1 and C2 (layer c).

For characterization of the dilution model, C3 and C4 were blocked, reagents were injected into the microfluidic system from C1 and C2, then flowed through concentration gradient generator and reaction chambers to C5. Furthermore, the effect of the flow rate was investigated by injecting H₂O₂ solutions into inlets C1 and C2 respectively, working reagent (L-tyrosine/HRP) was pumped into C3 and C4, after mixing and reacting, the fluorescence product was removed from C5. In surface modification process, all reagents were injected into the microfluidic system from C1 and C2, ultrapure water was injected into the micro-channel from C5 at the same flow velocity, waste was discarded via C3 and C4. During the enzyme activity detection process, substrate ACh (or ACh mixed with inhibitor in inhibition assay) was injected into the system from C1 and C2 to generate concentration gradient and catalyzed by immobilized enzyme in reaction chambers. Working solutions was injected from C3 and C4, and then mixed with reaction product H₂O₂ through long sinuous microchannel by diffusion effect, the fluorescence strength of product in detection wells could be monitored by a microplate reader. The design of the chip in our experiment can automatically and efficiently conduct sampling, dilution, incubation, mixing, washing and detection for high-throughput enzyme inhibitor assay.

Figure 1

The microfluidic chip (Fig. 1B) utilized in this experiment was prepared in a fashion similar to the one described in previous report³⁷. First of all, the layout of

microchannels network were designed using CorelDraw X4 software by us (Fig. S1 (A)), and then the copper molds (Fig. S1 (B)) were fabricated through a precise embossing process using a computerized numerical control (CNC) engraving and milling machine (Beijing, China). Then the well-mixed PDMS (USA, Sylgard184 A and B in 10:1 ratio) after degasifying it in a vacuum chamber was poured onto the copper mold to give a fluidic layer containing the micro-channels transferred from the master. The fluidic layer was cured in an 65°C oven for 1 h and peeled off from the mould after curing. Then holes (2.5 mm diameter) were made by a drill at the inlet and outlet channels for access of reaction solutions. Two PDMS layers were made with different microstructures, and a glass slide was washed with ethanol and ultrapure water successively, followed by baking at 80°C for 1 h. For the sealing, the PDMS pieces and the glass were treated by oxygen plasma for 3 min in a plasma generator, and immediately sealed together to form an irreversibly bonded PDMS microchip on a glass slide after heating at 80°C for 2 h. Polyethylene tubes were used to further connect the main inlet with a syringe pump for sample delivery and washing.

Preparation of immobilized AChE / ChO reactors

Prior to modification, it was worth noting that ultrapure water was injected into the micro-channel from C5 during all treatment and washing steps described below. This operation was carried out under controlled conditions (maintaining the same flow velocity by a syringe pump) to avoid a spread of the reagent into the detection windows and modification. All reagents were injected into the microfluidic system

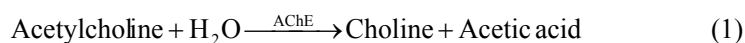
from C1 and C2, waste was discarded via C3 and C4.

The enzymes were chemically linked to the modified micro-channels similarly as described by Li et al³⁸. Firstly, the PDMS micro-channels were cleaned with ethanol and ultrapure water. Then, the microchip was oxidized by continuously passing a mixture of H₂O/H₂O₂/HCl (in a volume ratio of 5:1:1) for 30 min at room temperature to introduce hydrophilic surface³⁹, followed by rinsing with water for 20 min and with pure ethanol for 10 min successively at a flow rate of 20 μL·min⁻¹. Sequentially, the hydrophilic micro-channels were treated with 3% solution of various mixtures of 3-APTES and MTES (3:2,v/v) in absolute ethanol for 5 h at 65 °C to form a self-assembled monolayer. The unreacted silane mixtures were washed from the micro-channels by ethanol, and then placed in an oven at 90 °C for 1 h to give the amino-functionalized micro-channels. The chip was stored overnight at room temperature. 1% (v/v) glutaraldehyde solution as a cross-linker was pumped into the alkylamine-derivatized micro-channels at a flow rate of 5 μL·min⁻¹ for 2 h, followed by thoroughly rinsing with PBS (pH 7.0) buffer. The aldehyde functionalized micro-channels were filled with a mixture solution of AChE and ChO (pH 8.0), and kept overnight at 4 °C for immobilization. Following this reaction, the micro-channels were filled with 50 mM Tris·HCl buffer (pH 7.0) for 2 h to block the residual aldehyde groups. Finally, the immobilized bi-enzymes microchip was thoroughly washed with 0.01 MPBS (pH 7.4) and stored at 4 °C when not in use.

Activity and inhibitor assays with the immobilized and free enzyme

The assay was performed by indirectly using L-tyrosine, a sensitive fluorogenic

probe for H₂O₂. ACh was first hydrolysed to produce choline and acetate in the presence of AChE (see Eq. (1)). Subsequently, ChO could further oxidized choline to form betaine and H₂O₂ (see Eq. (2)), and then the latter reacted with the non-fluorescent substrate L-tyrosine to generate fluorescent dimer in the presence of HRP (see Eq. (3)), which exhibited strong fluorescence at 416 nm with an excitation wavelength of 320 nm. The fluorescence intensity of tyrosine dimer was directly proportional to the concentration of the H₂O₂, and partly reflected enzyme activity. Therefore, the change in the fluorescence intensity was employed to analyze enzyme inhibitors. These tandem reactions were represented according to the following equations.



$$\lambda_{ex/em} = 320/416\text{nm}$$

The enzyme activity and inhibitor assays were carried out in prepared microchip device and described below briefly. Substrate ACh (or ACh mixed with Donepezil in inhibition assay) was injected into the system from C1 and C2 (high and low concentration) to generate concentration gradient and catalyzed by immobilized enzyme in reaction wells. After incubation for 10 min, L-tyrosine/HRP mixture solution was injected from C3 and C4, and then mixed with product H₂O₂ through long sinuous micro-channels. Finally, the fluorescent dimer in detection chambers was quantified after 5 min.

The kinetic and activity assays of free form were implemented using a 96-well

microplate. The final assay volume used per well was 200 μL , with a reaction solution comprising final concentrations of 1 mM L-tyrosine, 3 $\text{U}\cdot\text{mL}^{-1}$ HRP, 0.03 $\text{U}\cdot\text{mL}^{-1}$ AChE and ChO, and a concentration range of ACh (0.005~10 mM) in assay buffer. The microplate was shaken for 0.1 min followed by reading the fluorescence at 1 min intervals for 60 min. For the inhibition assay, under the same condition, 2 μL of 3 $\text{U}\cdot\text{mL}^{-1}$ AChE solution was added to each well and incubated at 25°C for 10 min either in the presence or absence of inhibitor with the substrate ACh at a fixed concentration. Then the L-tyrosine/HRP/ChO working solutions were added to initiate the reaction. The fluorescence density of each well was simultaneously recorded after 15 min delay.

The percentage of inhibition for each inhibitor concentration was calculated by comparing the fluorescence intensity with those obtained in the absence of inhibitor, according to the following expression: $100 - (X/X_0 \cdot 100)$, where X was the fluorescence intensity obtained in the presence of the inhibitor, and X_0 was the fluorescence intensity obtained with the substrate solution only. The assays were carried out in triplicate, K_m and V_{\max} values were derived from Lineweaver and Burk reciprocal plot, and IC_{50} value was extrapolated graphically from inhibition curves (log inhibitor concentration vs percent of inhibition). All experiments were performed at room temperature $25 \pm 2^\circ\text{C}$, the normalized fluorescence was relative value by subtracting the intensity obtained in negative control .

Results and discussion

Characterization of the Dilution Model

Prior to the experiments, the performance of the dilution module was characterized. First, we used the relative simple and fast method to evaluate the concentration gradient preliminarily, as described previously⁴⁰. Fluorescein sodium ($E_x = 490$ nm, $E_m = 515$ nm) was used as a fluorescence probe to evaluate the gradient produced by the dilution module. Low ($0 \mu\text{M}$) and high ($2 \mu\text{M}$) concentrations of fluorescein sodium solution were injected into inlets C1 and C2 to C5 respectively, at a flow rate of $10 \mu\text{L} \cdot \text{min}^{-1}$ using a syringe pump, while C3 and C4 were blocked. Different concentrations of fluorescein sodium were formed gradually while passing the micro-channels and were quantified in detection chambers by a microplate reader. The corresponding theoretical fluorescence intensities were obtained by injecting six different concentration ($0, 0.4, 0.8, 1.2, 1.6, 2 \mu\text{M}$) into the two inlets of dilution module sequentially. The theoretical concentration values were calculated according to the equation (4) below described by Yang's group⁴¹:

$$C(i, N) = \frac{(N-i)C1}{N} + \frac{iC2}{N} \quad (4)$$

As shown in Fig. 1C, where $C(i, N)$ was the final concentration of distribution, C1 and C2 represented the initial concentration of reagent solution, N was the number of sequence of micro-channel and i stood for the number of sequence of branch point. Before the next experiments, the chip was washed three times with ethanol and water respectively to avoid possible interference. The datum analysis from Fig. 2A indicated that there was a good correlation between the theoretical and experimental data. The linearity of the six concentrations was good with coefficient of more than 0.99, proving the capability of this chip to generate linear concentration gradients.

In our work, the effect of injection flow velocities on a linear concentration gradient and the diffusive mixing were investigated. Then, Five flow velocities (2.5, 5, 10, 15, 20 $\mu\text{L}\cdot\text{min}^{-1}$) of solution were chosen in experiment. Similarly, low (0 μM) and high (20 μM) concentration of H_2O_2 solution were injected into inlets C1 and C2, respectively. Solutions were distributed and mixed gradually while moving through microchannels, six different concentrations of H_2O_2 solution were generated and then reacted with working reagent (L-tyrosine/HRP) delivered by fluid equivalent distribution channels. The fluorescent products in detection chambers were monitored. The comparison curve between the theoretical and the experimental data on the fluorescence intensity was shown in Fig.2B. When the flow velocity was lower than 10 $\mu\text{L}\cdot\text{min}^{-1}$, the experimental error against the theoretical intensity was acceptable since the mean relative deviation was below 5%, and the linearity of the six concentrations was good with coefficients of more than 0.993. Greater deviation occurred with the flow velocity increased. The variance was mainly attributed to the roughness of microchannel surface, which generate resistance to the liquid moving through the microchannels, the faster flow velocity may lead to the larger resistance, unequally mixing and incompletely reaction between substrate and enzyme as well as product and working reagent. Therefore, a flow rate of 10 $\mu\text{L}\cdot\text{min}^{-1}$ was chosen for sample injection to shorten analysis time and ensure reliable experimental results.

Figure 2

Optimization of measurement conditions in the microdevice

In our fluorescent reaction system, the pH value, type and concentration of the

buffer solution and reaction time were very important for the final detection sensitivity, because it have effected on the enzyme-catalyzed reaction and the fluorescence quantum yield. Thus, the optimal measurement conditions in experiments were investigated by using 0.04 and 0.08 mM of H₂O₂ solutions as samples, respectively. H₂O₂ solution via inlets C1 and C2, working reagent (L-tyrosine/HRP) via inlets C3 and C4 were loaded into channels at a flow velocity of 10 $\mu\text{L}\cdot\text{min}^{-1}$.

Different mixed solutions were prepared by using the PB solution with different pH values, and then the pH was investigated. Obtained result was shown in Fig. 3. As already reported⁴², the optimum pH values for AChE and ChO were pH 8.0~9.0 and 7.0~8.0 respectively, given the maximum biocatalytic activity of two enzymes and detection sensitivity, a pH 8.0 value was chosen in the following experiments.

Figure 3

Meanwhile, the effect of different buffer type on the fluorescent signal was also studied in the microdevice. The pH values of the mixed solutions were adjusted to 8.0 by using 0.05 M of PB and Tris·HCl buffer solution respectively, and their fluorescence intensities were quantified (Fig. 4a). The observed results showed that fluorescence intensities of PB were higher than Tris buffer solution. Hence, PB buffer solution was selected in the experiment.

Besides, to further improve the detection sensitivity, we also carefully tested the influences of the concentration of phosphate buffer solution (10~200 mM). The fluorescent signal of dimer significantly increased with the increase of the

concentration of the phosphate buffer solution till 50 mM, and then it decreased gradually (Fig. 4b). Results suggested that the concentration of phosphate buffer can severely affect enzyme activity and fluorescence quantum yield. Lower buffer concentration has the most stabilizing effect on enzyme, and concentrated buffer can contribute significantly to avoiding HRP suicide inactivation in the presence of excessive H₂O₂. The consequence was generally good agreement with previous reports^{43, 44}. Above all, 50 mM of phosphate buffer solution was employed for all further experiments.

Figure 4

The fluorescence intensity and stability were also monitored with time, as shown in Fig. 5. Experimental result revealed that L-tyrosine was converted into a fluorescent dimer in the presence of HRP and H₂O₂, and the reaction was completed within 1 min (Fig. 2S). In addition, the fluorescence intensity was stable for at least several minute. To meet the requirements of experimental operation, 5 min was chosen as a reaction time. All of these results illuminated that the fluorescence reaction system has a better response and stability under the optimum conditions.

Figure 5

Immobilized and free enzyme assays

The global activity of the immobilized enzymes in our microchip was measured before the enzyme inhibitor assay. Under the optimum conditions, the kinetic parameters were investigated by sequentially injecting ACh solution with a concentration range of 0.02 to 2 mM into the micro-channels (Fig. 6). ACh was

converted into the end product H_2O_2 by immobilized enzymes, the incubation was completed within 10 minutes. The calibration curve between the fluorescence intensity and the concentrations of ACh was linear, and the correlation was found to be 0.991 in the range from 0.02 to 0.2 mM (Fig. 6, inset), and the mean RSD for the replicates was 6.1%. Moreover, the LOD was calculated as 1.4×10^{-2} mM for acetylcholine which was higher than the conventional method (1.2×10^{-3} mM). It was clear that the top PDMS layer might have a slight effect on the fluorescence detection. However, the microfluidic system provided a sealed environment, which could reduce the possible opportunities for contamination. Furthermore, the LOD value was sufficient for the further applications and did not affect the inhibitor analysis in our work. Further studies can be focused on improve sensitivity of the device by using better transparency material or detection system. The kinetic constants of K_m and V_{\max} were derived from the Lineweaver-Burk by plotting velocity (micromoles of product formed per minute) versus normalized substrate concentration (Table 1). The K_m value of 376.33 ± 32.0 μM for immobilized AChE/ChO was sixfold higher than the value of 58.81 ± 2.92 μM for free from in solution, indicating that the immobilization procedure decreased the affinity of the enzyme for the substrate, which may be caused by the diffusional resistance of the substrate to the bound enzyme²⁴. Nevertheless, the K_m value of immobilized AChE/ChO was lower than the reported one²³, showing that this study could provide effective multienzyme immobilization method for improving the affinity of an enzyme to its substrate. Furthermore, the V_{\max} of free AChE/CHO in solution was found to be 208.33 ± 9.50 $\Delta\text{F} \cdot \text{min}^{-1}$ while it was 101.56 ± 8.43 $\Delta\text{F} \cdot \text{min}^{-1}$

(2.05-fold decrease) for immobilized enzymes system. It could be that the deactivation of the enzymes after immobilization. However, the enzymatic activity was maintained and can be used for enzyme inhibition assay.

Figure 6

Table 1

Summary of parameters obtained from microchip and microplate based on the fluorescence assay and comparison with reference method.

Parameters	Immobilized AChE-CHO	Free AChE-CHO	Reference method
K_m (μM)	376.33 ± 32.0	58.81 ± 2.92	-
V_{\max} ($\Delta F \cdot \text{min}^{-1}$)	101.56 ± 8.43	208.33 ± 9.50	-
IC_{50} (nM)	32.35 ± 1.03	27.48 ± 1.05	6 ~ 48

The IC_{50} of Donepezil was obtained by the simultaneous injection of a single initial inhibitor concentration with the fixed concentration of ACh into the bi-enzymes system. Reduced relative fluorescence intensity was closely correlated to inhibition of the enzymatic activity (Fig. 7). The percentage of inhibition versus inhibitor concentration was fitted using the GraphPad Prism 5.0 to obtain the IC_{50} value, based on the sigmoidal dose response curve⁴⁵. The IC_{50} value (32.35 ± 1.03 nM) extrapolated and normalized with the immobilized enzymes was comparable to the literature reported values by using Ellman's colorimetric assay that estimated between 6 and 48 nM^{46, 47}, a delicate difference could be due to the different experimental conditions and measurement method. Moreover, IC_{50} value of the immobilized bi-enzymes microchip was found similar (same order of magnitude) to the value

(27.48 ± 1.05 nM) of free form in solution, which could confirm the fact that the AChE/ChO immobilized microfluidic chip for inhibition assay was reliable. Besides, in comparison, the traditional microplate methods took about 25 min and 200 μ L reagents for the determination of the inhibition of one sample, while the microfluidic enzyme inhibition assay took only about 18 min and required 15 μ L reagents due to rapid diffusing and mixing on miniature chip. What's more, six measurements were achieved in parallel with a sample injection (equivalent to six wells in microplate analysis). The short analysis time and less reagent consumption showed that the microchip will be a promising potential microfluidic analytical platform for inhibitor screening.

Figure 7

Conclusions

In this research, a miniaturized three-layer PDMS-based microfluidic system was prepared for enzyme inhibition assay successfully. Enzyme kinetic parameters of immobilized and free form were investigated and the results proved that the enzymes can be successfully immobilized with retention of its activity. Moreover, the analytical condition was optimized, including buffer (pH, types and concentration), substrate concentration, reaction time. The obtained IC_{50} value of Donepezil was found in agreement with those derived by the traditional microplate method as well as the literature data, which revealed that the inhibition assay in immobilized enzyme microfluidic chip was reliable. Although the detection limit of acetylcholine was

slightly higher than traditional method, which was sufficient for the inhibitor analysis in our work. Further studies can be focused on explore and improve sensitivity of the device compared with the existing method. However, the co-immobilized enzymes microchip analysis platform described here has the advantages of lower costs, short analysis time, less reagent consumption and automation, which can be applied to analyze enzyme inhibitor quickly and easily. Hence, it will be a promising and effective microfluidic tool for screening of AChEIs.

Acknowledgments

This work was financially supported by the National Natural Science Foundation of China (No. 20875105)

References

1. M. Singh, M. Kaur, H. Kukreja, R. Chugh, O. Silakari and D. Singh, *European Journal of Medicinal Chemistry*, 2013, **70**, 165-188.
2. R. M. Lane, S. G. Potkin and A. Enz, *International Journal of Neuropsychopharmacology*, 2006, **9**, 101-124.
3. H. Dvir, I. Silman, M. Harel, T. L. Rosenberry and J. L. Sussman, *Chemico-Biological Interactions*, 2010, **187**, 10-22.
4. L. Anglister, A. Etlin, E. Finkel, A. R. Durrant and A. Lev-Tov, *Chemico-Biological Interactions*, 2008, **175**, 92-100.
5. H. M. Greenblatt, H. Dvir, I. Silman and J. L. Sussman, *Journal of Molecular Neuroscience*, 2003, **20**, 369-383.
6. M. Pohanka, *Biomedical Papers-Olomouc*, 2011, **155**, 219-229.
7. P. Raina, P. Santaguida, A. Ismaila, C. Patterson, D. Cowan, M. Levine, L. Booker and M. Oremus, *Annals of Internal Medicine*, 2008, **148**, 379-W385.
8. C. G. Parsons, W. Danysz, A. Dekundy and I. Pulte, *Neurotoxicity Research*, 2013, **24**, 358-369.
9. H. Q. Lin, M. T. Ho, L. S. Lau, K. K. Wong, P. C. Shaw and D. C. C. Wan, *Chemico-Biological Interactions*, 2008, **175**, 352-354.
10. L. Huang, T. Su and X. S. Li, *Current Topics in Medicinal Chemistry*, 2013, **13**, 1864-1878.
11. F. Arduini, A. Amine, D. Moscone and G. Palleschi, *Microchim Acta*, 2010, **170**, 193-214.
12. Y. Q. Miao, N. Y. He and J. J. Zhu, *Chemical Reviews*, 2010, **110**, 5216-5234.
13. G. L. Ellman, K. D. Courtney, V. Andres jr and R. M. Featherstone, *Biochemical Pharmacology*, 1961, **7**, 88-95.
14. K. A. Askar, A. C. Kudi and A. J. Moody, *Can J Vet Res*, 2011, **75**, 261-270.
15. D. Dingova, J. Leroy, A. Check, V. Garaj, E. Krejci and A. Hrabovska, *Anal Biochem*, 2014, **462**, 67-75.
16. A. Khan and S. Ab Ghani, *Biosens Bioelectron*, 2012, **31**, 433-438.
17. F. E. Kanik, M. Kolb, S. Timur, M. Bahadir and L. Toppare, *Int J Biol Macromol*, 2013, **59**, 111-118.
18. N. Chauhan and C. S. Pundir, *Biosens Bioelectron*, 2014, **61**, 1-8.
19. L. Betancor and H. R. Luckarift, *Biotechnol Genet Eng*, 2010, **27**, 95-114.
20. R. C. Rodrigues, C. Ortiz, A. Berenguer-Murcia, R. Torres and R. Fernandez-Lafuente, *Chem Soc Rev*, 2013, **42**, 6290-6307.
21. T. Chovan and A. Guttman, *Trends in Biotechnology*, 2002, **20**, 116-122.
22. S. Matosevic, N. Szita and F. Baganz, *Journal of Chemical Technology and Biotechnology*, 2011, **86**, 325-334.
23. P. He, J. Davies, G. Greenway and S. J. Haswell, *Analytica Chimica Acta*, 2010, **659**, 9-14.
24. J. I. da Silva, M. C. de Moraes, L. C. C. Vieira, A. G. Correa, Q. B. Cass and C. L. Cardoso, *Journal of pharmaceutical and biomedical analysis*, 2013, **73**, 44-52.
25. S. R. Lee, H. E. Lee, Y. O. Kang, W. S. Hwang and S. H. Choi, *Advances in Materials Science and Engineering*, 2014, DOI: 10.1155/2014/971942.
26. E. Aynaci, A. Yasar and F. Arslan, *Sensors and Actuators B-Chemical*, 2014, **202**, 1028-1036.
27. M. Vandeput, C. Parsajoo, J. Vanheuverzwijn, S. Patris, Y. Yardim, A. le Jeune, A. Sarakbi, D.

-
- Mertens and J. M. Kauffmann, *Journal of pharmaceutical and biomedical analysis*, 2015, **102**, 267-275.
28. F. Rusmini, Z. Y. Zhong and J. Feijen, *Biomacromolecules*, 2007, **8**, 1775-1789.
29. A. Caro, V. Humblot, C. Methivier, M. Minier, L. Barbes, J. Li, M. Salmain and C. M. Pradier, *Journal of Colloid and Interface Science*, 2010, **349**, 13-18.
30. N. R. Glass, R. Tjeung, P. Chan, L. Y. Yeo and J. R. Friend, *Biomicrofluidics*, 2011, **5**.
31. P. Zucca and E. Sanjust, *Molecules*, 2014, **19**, 14139-14194.
32. K. S. Deshpande, S. Kuddannaya, J. Stagnus, P. C. Thune, L. de Smet, J. H. ter Horst, L. A. M. van der Wielen and M. Ottens, *Biochemical Engineering Journal*, 2012, **67**, 111-119.
33. N. S. K. Gunda, M. Singh, L. Norman, K. Kaur and S. K. Mitra, *Applied Surface Science*, 2014, **305**, 522-530.
34. N. Aissaoui, L. Bergaoui, J. Landoulsi, J. F. Lambert and S. Boujday, *Langmuir*, 2012, **28**, 656-665.
35. Z. H. Wang and G. Jin, *Colloids and Surfaces B-Biointerfaces*, 2004, **34**, 173-177.
36. D. K. Goyal and A. Subramanian, *Thin Solid Films*, 2010, **518**, 2186-2193.
37. D. P. Sun, J. Lu, Z. G. Chen, Y. Y. Yu and Y. B. Li, *Microfluid Nanofluid*, 2014, **17**, 831-842.
38. Y. S. Li, W. P. Liu, X. F. Gao, D. D. Chen and W. G. Li, *Biosens Bioelectron*, 2008, **24**, 538-544.
39. G. D. Sui, J. Y. Wang, C. C. Lee, W. X. Lu, S. P. Lee, J. V. Leyton, A. M. Wu and H. R. Tseng, *Anal Chem*, 2006, **78**, 5543-5551.
40. D. Gao, H. F. Li, N. J. Wang and J. M. Lin, *Anal Chem*, 2012, **84**, 9230-9237.
41. F. Yang, Z. G. Chen, J. B. Pan, X. C. Li, J. Feng and H. Yang, *Biomicrofluidics*, 2011, **5**.
42. X. Gao, G. C. Tang and X. G. Su, *Biosens Bioelectron*, 2012, **36**, 75-80.
43. L. Haifeng, L. Yuwen, C. Xiaomin, W. Zhiyong and W. Cunxin, *Journal of Thermal Analysis and Calorimetry*, 2008, **93**, 569-574.
44. S. Asad, S. F. Torabi, M. Fathi-Roudsari, N. Ghaemi and K. Khajeh, *Int J Biol Macromol*, 2011, **48**, 566-570.
45. S. Q. Gu, Y. L. Lu, Y. P. Ding, L. Li, F. F. Zhang and Q. S. Wu, *Analytica Chimica Acta*, 2013, **796**, 68-74.
46. N. Guzior, M. Bajda, J. Rakoczy, B. Brus, S. Gobec and B. Malawska, *Bioorgan Med Chem*, 2015, **23**, 1629-1637.
47. P. Meena, V. Nemaish, M. Khatri, A. Manral, P. M. Luthra and M. Tiwari, *Bioorgan Med Chem*, 2015, **23**, 1135-1148.

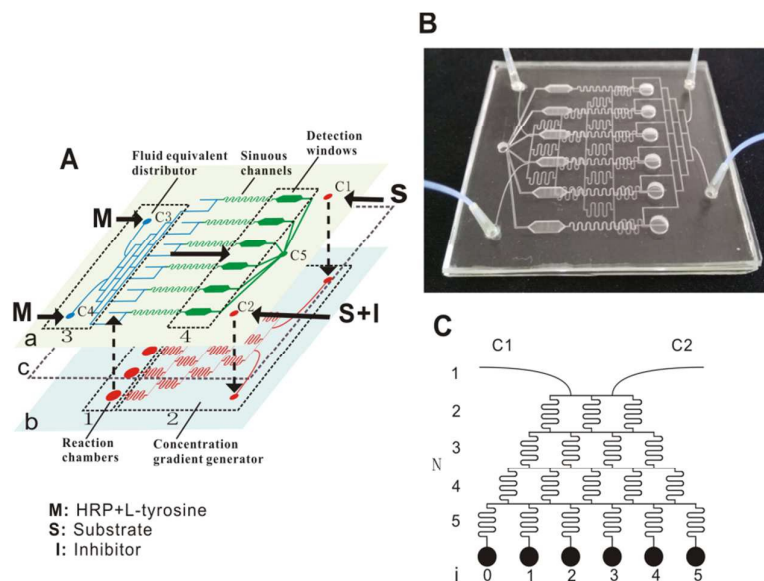


Fig. 1 Integrated microfluidic chip for AChEIs assay. (A) The main functional unit of the microchip include: reaction chambers (part 1, 3.0 mm diameter, 1.5 mm high, 10 μ L volume); concentration gradient generator (part 2, 150 μ m width, 100 μ m depth); a fluid equivalent distributor (part 3, 150 μ m width, 100 μ m depth); fluorescence derivation channels and detection windows (part 4, 3.0 mm wide, 5.0 mm long, and 1.0 mm high). (B) A real image of a microfluidic device that containing functional parts. (C) The concentration gradient generator with reaction wells on layer b.

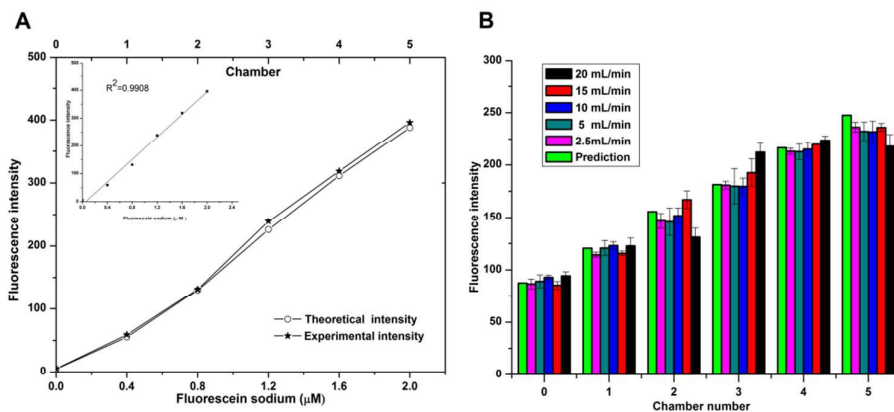


Fig. 2 The comparison between the theoretical and the experimental data on the fluorescence intensity generated by the dilution model. (A) The preliminary availability evaluation of microchip. Inset is a linear fit derived from experimental data (fluorescence probe: 0 and 2 μM fluorescein sodium). (B) Effect of the flow velocities on concentration gradient. Error bars represent the standard deviations of measurements. ($n = 3$).

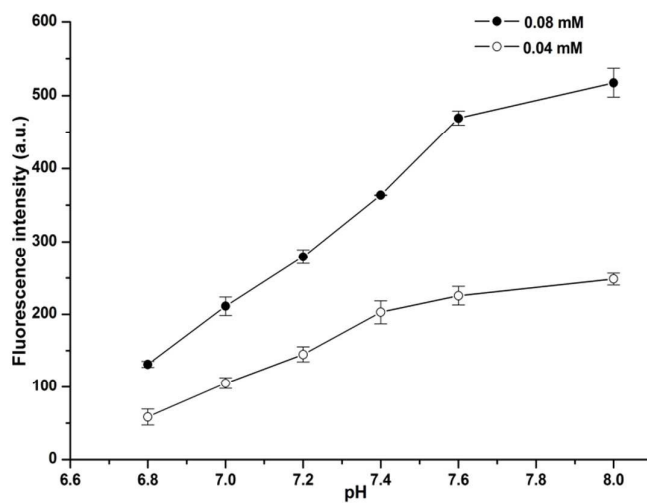


Fig. 3 Effect of pH of reaction solution on fluorescence intensity, using H_2O_2 solutions with concentrations of 0.04 mM (○) and 0.08 mM (●). Error bars represent the standard deviations of measurements. ($n = 3$)

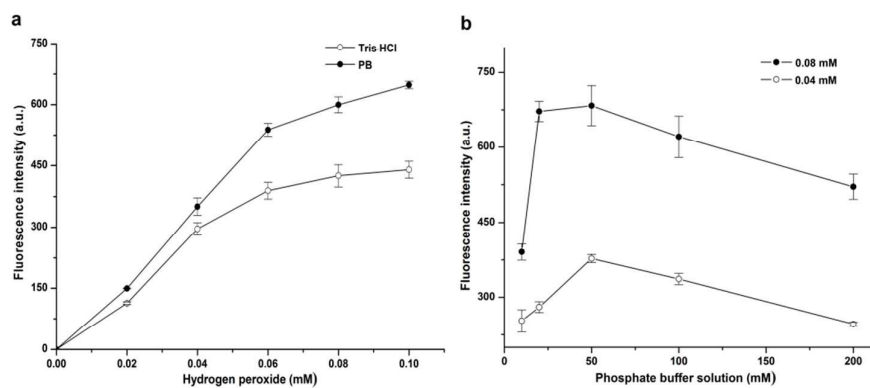


Fig. 4 Effect of the buffer type (a) and phosphate buffer concentration (b) on fluorescence intensity. Error bars represent the standard deviations of measurements ($n = 3$).

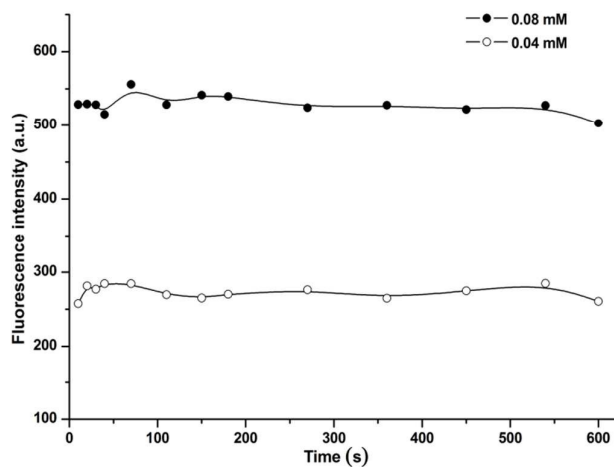


Fig. 5 The stability of fluorescence intensity against time, using H_2O_2 solutions with concentrations of 0.04 mM (\circ) and 0.08 mM (\bullet).

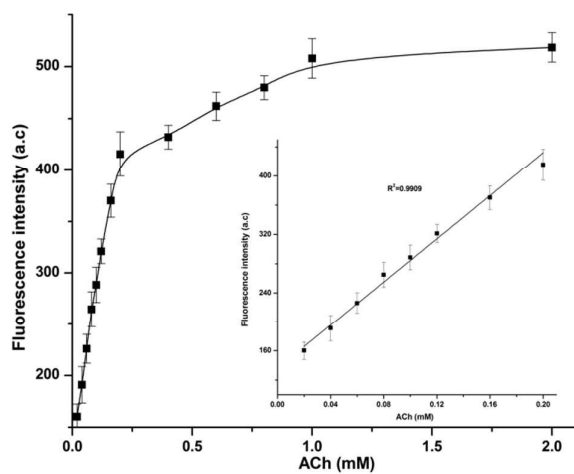


Fig. 6 Fluorescence intensity in relation to concentration of ACh. The line in the inset is a linear fit. Error bars represent the standard deviations of measurements ($n = 3$).

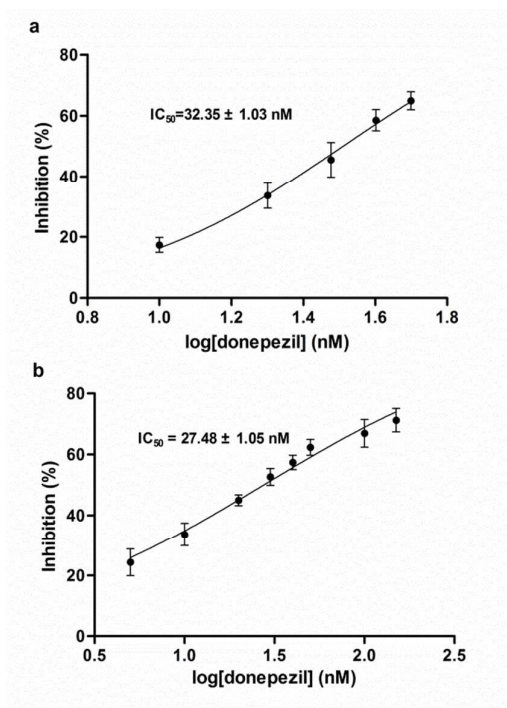


Fig.7 Inhibition curves for Donepezil using the microfluidic device (a) and 96-well microplate (b). Error bars represent the standard deviations of measurements (n = 3).